Assessment of mechanical, thermal, and sliding wear performance of chemically treated alumina-filled biocomposites using machine learning and response surface methodology

Article *in* Polymer Composites · March 2025

DOI: 10.1002/pc.29798

4 authors, including:

Shaisundaram V S
Vels University
42 PUBLICATIONS **622** CITATIONS
SEE PROFILE

Saravanakumar Sengottaiyan
Easwari Engineering College
32 PUBLICATIONS **310** CITATIONS
SEE PROFILE

Received: 24 January 2025 | Revised: 3 March 2025 | Accepted: 5 March 2025

DOI: 10.1002/pc.29798

RESEARCH ARTICLE

Polymer COMPOSITES WILEY

Assessment of mechanical, thermal, and sliding wear performance of chemically treated alumina-filled biocomposites using machine learning and response surface methodology

V. S. Shaisundaram[1] | **Saravanakumar Sengottaiyan**[2] | **Rajesh Mohan**[3] | **Vishnupriya Gurunathan**[4]

[1]School of Engineering, Vels Institute of Science Technology and Advanced Studies, Chennai, India

[2]Faculty of Engineering and Technology, Villa College, Male, Maldives

[3]Department of Mechanical Engineering, Karpagam College of Engineering, Coimbatore, India

[4]Department of Computer Science and Engineering, Easwari Engineering College, Chennai, India

Correspondence
Saravanakumar Sengottaiyan, Faculty of Engineering and Technology, Villa College, Male 20002, Maldives.
Email: s.sengottaiyan@villacollege.edu.mv

Abstract

This study examines how NaOH treatment and alumina filler affect the mechanical properties, water absorption, thermal degradation, and sliding wear of epoxy composites reinforced with pineapple leaf fiber. NaOH treatment greatly improved the composites' tensile, flexural, and impact strengths by strengthening the bond between the fiber and matrix. Furthermore, the incorporation of alumina filler further elevated the mechanical properties. The composite with 10% alumina showed peak values of 41.4 MPa in tensile strength, 63.8 MPa in flexural strength, and 37.6 kJ/m^2 in impact strength. Because hygroscopic parts were removed from the treated composites, they absorbed much less water. The 15% alumina composite had the lowest absorption at 18% after 192 h. Thermal degradation analysis showed that NaOH treatment improved thermal stability, with the 15% alumina composite having the highest char residue (15.3%) at 700°C. Sliding wear tests showed that alumina reinforcement significantly reduced specific wear rate (SWR) and coefficient of friction (COF). The improved 15% alumina composite had an SWR of 0.2598×10^{-5} mm^3/Nm and a COF of 0.103 when sliding at 120 cm/s, with a 45 N load and over 1500 m of distance. A scanning electron microscopy study found that untreated composites experienced severe abrasive wear, while treated and reinforced composites exhibited mild adhesive wear. The study shows that treating PALF composites with NaOH and adding alumina enhance their mechanical, thermal, and tribological properties, making them suitable for high-performance industrial applications.

Highlights

- Alumina filler improved tensile (41.4 MPa) and flexural strength (63.8 MPa).
- NaOH-treated composites absorbed 18% less moisture, enhancing durability.
- Thermal stability improved, with 15.3% char residue at 700°C for 15% alumina.
- Optimized composite achieved the lowest wear rate (0.2598×10^{-5} mm^3/Nm).
- Artificial neural network and response surface methodology accurately predicted and optimized composite wear behavior.

KEYWORDS

alumina reinforcement, machine learning, pineapple leaf fiber, sliding wear, thermal stability

1 | INTRODUCTION

Natural fibers are gaining attention as eco-friendly alternatives to synthetic fibers in polymer composites due to their benefits like biodegradability, availability, cost-effectiveness, and lightweight properties.[1–3] These fibers, often made from agricultural waste, reduce environmental harm and promote the use of renewable resources.[4–6] Natural fiber-reinforced composites provide eco-friendly materials for modern industries, aligning with global sustainability goals by transforming waste into valuable products.[7–9] Natural fiber composites are increasingly used in the automotive, construction, and packaging industries because they are sustainable, lightweight, and have beneficial mechanical properties.[10–12] Despite their advantages, natural fibers possess inherent drawbacks that hinder their overall performance.[13,14] Weak bonding between hydrophilic natural fibers and hydrophobic polymer matrices often reduces mechanical strength due to poor compatibility.[15] Furthermore, the poor heat stability and excessive moisture absorption of natural fibers limit their use in demanding conditions. Chemical treatments such as alkali therapy, particularly with sodium hydroxide (NaOH), are employed to tackle these challenges effectively.[16,17] Studies have examined natural and agricultural fibers, including Ficus benghalensis, rice stubble, basalt, and jute, along with ceramic fillers to improve the mechanical and tribological properties of polymer composites.[18–20] Research has demonstrated that hybrid composites exhibit improved wear resistance, thermal stability, and structural integrity under varying conditions.[21–24]

Alkali treatment increases fiber surface roughness and enhances their bonding with the polymer matrix by removing contaminants like lignin, hemicellulose, and wax.[25–27] In addition to increasing composites' mechanical performance, this treatment lowers moisture absorption and enhances dimensional stability.[28,29] Furthermore, adding ceramic fillers like alumina has demonstrated significant promise for improving tribological, mechanical, and thermal characteristics.[30,31] Alumina is an excellent choice for reinforcing polymer matrices due to its high hardness, thermal stability, and wear resistance.[32–34] PALF was selected as a reinforcing material because of its strong mechanical properties, sustainability, and abundance as agricultural waste.[35,36] PALF has about 80% cellulose, which improves fiber-matrix interactions and increases tensile and flexural strength when chemically treated. PALF has a higher specific strength, low density, and good thermal stability than other natural fibers, making it suitable for lightweight composites. Additionally, PALF is abundant, cost-effective, and biodegradable, making it an eco-friendly alternative to synthetic fibers.[37–39] Chemical treatment of PALF with NaOH enhances fiber-matrix adhesion, lowers moisture absorption, and improves interfacial bonding, resulting in better composite mechanical and tribological performance. PALF was chosen to create a high-performance composite material for industrial use that offers improved mechanical strength, wear resistance, and durability.[40,41] Alumina enhances the durability of composites in high-stress and high-friction applications due to its hardness and wear resistance, improving tribological performance.[42] This study aims to systematically investigate how NaOH treatment and alumina filler reinforcement influence the mechanical, thermal, water absorption, and sliding wear properties of PALF-reinforced epoxy composites. The study focuses on improving natural fibers by optimizing their treatment and filler content, creating a high-performance and sustainable composite for industrial uses such as equipment, buildings, and automobiles. This strategy not only enhances the utility of agricultural waste but also encourages the development of eco-friendly materials with better performance.

Recent studies have examined how adding PALF and ceramic fillers to polymer composites can improve their mechanical, thermal, and wear properties. According to Saha et al.,[43] 2.5% of content increased impact strength (88.63 J/m), whereas 7.5% PALF particles maximized tensile strength (89.43 MPa) and fracture toughness (4.54 MPa $m^{1}/^{2}$). Praveena et al.[44] found that adding 40% PALF to polyester composites raised tensile strength to 66 MPa and Young's modulus to 2545 MPa, highlighting the importance of fiber content for strengthening fiber-matrix bonds. The significance of chemical treatments for fiber compatibility was highlighted by Gnanasekaran et al.'s[45] findings that alkali-treated PALF, specifically with 8% NaOH, increased tensile strength (116 MPa) and decreased water absorption to 6%. Senthilkumar et al.[46] confirmed this by showing that NaOH and KOH treatments reduced fiber pull-out and increased the tensile modulus to 1.78 GPa. 15% NaOH-treated fibers showed better wear resistance, reducing specific wear rate (SWR) and coefficient of friction (COF), as Rajeshkumar et al.[47] showed. Santhosh Nagaraja et al.[48] and Sabarinathan et al.[49] highlighted that using 6% fly ash (FA) and 20%

recovered brown alumina (RBA) fillers significantly improved mechanical properties and water resistance.

Despite these advancements, limited research has focused on combining alumina fillers with PALF treated with NaOH to optimize its mechanical, water absorption, thermal, and tribological properties. The majority of current research optimizes either fiber treatment or filler alone without considering their combined benefits. This study combines NaOH-treated PALF with various amounts of alumina filler in epoxy composites to enhance all qualities equally. The breakthrough is the simultaneous enhancement of wear resistance by alumina reinforcement and fiber-matrix adhesion through alkali treatment. The study systematically evaluates the effects of treatment and filler on mechanical, thermal, water absorption, and sliding wear properties. This study addresses previous research gaps and offers new insights into developing high-performance, sustainable PALF-based composites for industrial use.

2 | MATERIALS AND METHODS

2.1 | Materials

PALF was sourced from agricultural regions and processed using a fiber extraction system at Easwari Engineering College in Chennai, India. The extracted fibers were treated with a 5% NaOH solution (1 L of water) to effectively remove contaminants such as lignin and hemicellulose,[50] following established protocols from previous studies.[51,52] The chemical treatment enhanced the interfacial adhesion between the fibers and the epoxy matrix. The processed fibers were rinsed with distilled water to remove any alkali, neutralized to a pH of 7, and air-dried for 48 h. After drying, the fibers were trimmed to specified diameters to provide consistent reinforcement in the composite. The study used epoxy resin (LY556) and its hardener (HY951) for their strong mechanical properties and compatibility with natural fibers.[53] Alumina particles were chosen as a filler due to their exceptional hardness and thermal stability. These high-quality materials were sourced from the M/s Fiber Region in Chennai. The use of alumina particles was intended to improve the mechanical, thermal, and tribological characteristics of the composite.[54] The materials were selected to provide excellent composite performance while ensuring cost-effectiveness and sustainability, following the study's goals.

2.2 | Composite fabrication

Compression molding was used to ensure an even distribution of fibers and alumina fillers in the epoxy matrix (Figure S1). The required composite configurations were created by mixing specific ratios of PALF, alumina fillers, and epoxy resin, as detailed in Table 1. Five different kinds of laminates were made: untreated, treated, and composites loaded with alumina. The required amounts of epoxy resin, hardener, treated and untreated PALF, and alumina fillers were measured for the fabrication process. To ensure an even distribution of fibers and fillers within the matrix, the ingredients were thoroughly blended. Subsequently, the mixture was poured into a preheated mold measuring $300 \times 300 \times 3\ mm^3$. A compression molding machine provided a pressure of 20 bar while the mold was heated to 150°C. For 20 min, this temperature and pressure were kept constant to let the epoxy resin cure properly. For optimal polymerization, the cured composite plates were removed from the mold and allowed to air-cure for an additional 24 h.[55]

The proportions of PALF and epoxy were adjusted to accommodate alumina fillers while keeping the total weight percentage of the composite at 100%. To provide a balanced composition and constant mechanical characteristics, the fiber content was decreased and the epoxy content was kept at 65% for laminates with 5%, 10%, and 15% alumina. The filler content (5, 10, and 15 wt% alumina) was selected based on the author's previous studies on alumina-filled banana fiber composites, where these compositions significantly enhanced mechanical, thermal, and tribological properties. Extensive trials with different fiber and filler compositions were conducted, and optimization studies confirmed that this range provides the best reinforcement while maintaining fiber integrity.[54,56]

2.3 | Mechanical testing

Tensile, flexural, and impact tests were conducted to evaluate the mechanical properties of the composites (Figure S2). A UNITEK universal testing machine was used to perform tensile testing in compliance with ASTM D638-10 guidelines.[57] Tensile strength and elongation were tested on $165 \times 25 \times 3\ mm^3$ specimens at a crosshead speed of 5 mm/min. Flexural strength was measured using an Instron Model 3382 machine according to ASTM D790-07 standards. Flexural strength was measured by applying a load to specimens sized $125 \times 12.7 \times 3\ mm^3$ at a rate of 2.8 mm/min, with the maximum load documented. An impact resistance test was conducted using a Tinius Olsen impact tester, adhering to the ASTM D256-06 standards. Specimens measuring $65 \times 12.7 \times 3\ mm^3$ were tested for impact resistance by striking them with a pendulum and measuring the energy absorbed during fracture. The tests provided in-depth insights into the tensile, flexural, and impact properties of the composites.

TABLE 1 Laminates proportion.

S.No	Abbreviation	Description	Proportion (wt%)
1	UPALF	Untreated PALF+Epoxy	70% epoxy+30% UPALF
2	TPALF	Treated PALF+Epoxy	70% epoxy+30% TPALF
3	TPALF5	Treated PALF+Epoxy+Al_2O_3	65% epoxy+30% TPALF+5% Al_2O_3
4	TPALF10	Treated PALF+Epoxy+Al_2O_3	65% epoxy+25% TPALF+10% Al_2O_3
5	TPALF15	Treated PALF+Epoxy+Al_2O_3	65% epoxy+20% TPALF+15% Al_2O_3

2.4 | Water absorption behavior

The water absorption behavior of the composites was assessed by immersing the specimens in distilled water at room temperature for periods of 24, 48, 72, 96, and 120 h. The percentage weight gain was calculated using the formula[54]:

$$\text{Percentage of weight increased} = \frac{W_f - W_i}{W_f}, \quad (1)$$

where W_i is the specimen's beginning weight and W_f is its final weight. The specimens were taken out of the water after each immersion period, cleaned to get rid of any remaining surface moisture, and weighed on a precision scale with a minimum count of 0.1 mg. The hydrophilic behavior and resistance to moisture absorption of the composites were shown by this investigation.

2.5 | Thermal degradation behavior

A thermogravimetric analyzer (EXSTAR TG/DTA 6300) at Annamalai University's Department of Physics was used to study thermal degradation. The experiments took place in a nitrogen environment with a gas flow rate of 200 mL/min and a heating rate of 10°C/min, reaching a maximum temperature of 700°C. The weight loss during heating was monitored to assess the thermal stability and degradation of the composites. The gathered information helped identify char residue and breakdown temperatures, providing key insights into the thermal performance of the composites.

2.6 | Sliding wear behavior

The sliding wear behavior of alumina-filled PALF composites was tested using a pin-on-disc tribometer (CONMAT BA/0001 model), following ASTM G99 guidelines (Figure S3). To assess their tribological performance, composite samples of $8 \times 5 \times 3\ mm^3$ were put to the test against an EN24 steel disc with a hardness of 62 HRC.[58] The wear tests were carried out in a variety of settings using a three-level experimental design. The input factors included sliding distance (500, 1000, and 1500 m), sliding load (15, 30, and 45 N), sliding velocity (40, 80, and 120 cm/s), and alumina filler content (5%, 10%, and 15%), corresponding to the TPALF5, TPALF10, and TPALF15 samples. Previous research has identified parameter levels that, when experimentally validated, have a significant impact on sliding wear resistance. Studies have also demonstrated that these specific parameter levels yield optimal tribological properties, ensuring improved wear performance.[58,59] An optimal design from Design-Expert software was used to thoroughly cover the parameter space in 25 tests. The tests evaluated the wear resistance and friction of the composites by measuring the COF and SWR.[60] The experimental design offered a methodical way to comprehend the composites' tribological behavior. The effect of operating conditions and alumina filler content on wear resistance and friction was assessed by adjusting key parameters. This detailed experiment identified optimal conditions to reduce SWR and COF, offering valuable insights for potential technical and industrial applications of the composites.

2.6.1 | Prediction and optimization modeling

This study examined the mechanical, thermal, and wear properties of alumina-filled PALF-reinforced epoxy composites using artificial neural networks (ANNs) and response surface methodology (RSM) for prediction and optimization. The authors found that RSM and ANN offered the most accurate predictions for fiber-reinforced composites after testing simulated annealing and genetic algorithms.[61] RSM effectively captures parameter interactions and optimizes responses with fewer trials, whereas the ANN, fine-tuned through GridSearchCV, showcased outstanding predictive accuracy. The ANN model was developed in Python, where its architecture was optimized by adjusting hyperparameters such as batch size, epochs, and hidden layer neuron count through grid search.[62,63]

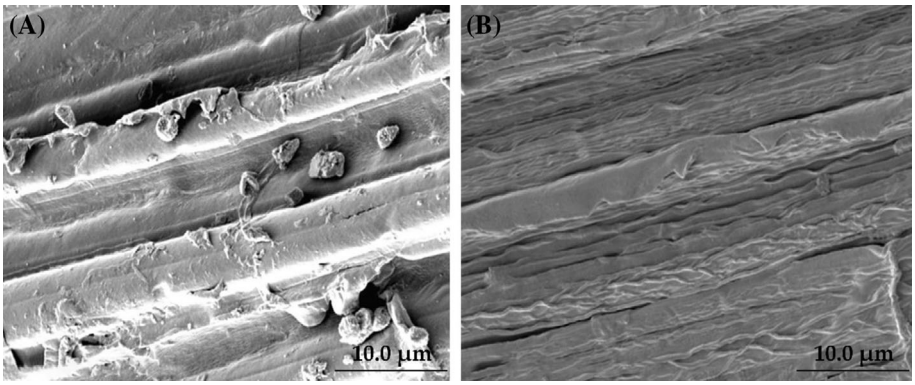

FIGURE 1 Scanning electron microscopy image of (A) UPALF and (B) 5% NaOH TPALF.

The model accurately predicted results during training, allowing us to explore the effects of parameters without needing more experiments based on the experimental data we collected. To reduce SWR and COF, input parameters were optimized through RSM in Design-Expert software, using a systematic three-level experimental design.[64,65] RSM generated a quadratic model, effectively capturing individual effects and interactions between parameters, allowing for statistical analysis and optimization.[66] The optimal RSM model involved 25 experimental runs to find the best combinations of sliding velocity, load, distance, and alumina content that minimize SWR and COF for improved performance. Combining RSM's statistical optimization with ANN's predictive abilities and Python-based hyperparameter tuning offers a well-rounded approach combining computational and experimental techniques. This approach systematically improved the composite's performance, producing reliable and robust results.

3 | RESULTS AND DISCUSSION

3.1 | Scanning electron microscopy characterization of untreated and 5% NaOH-TPALF

Scanning electron microscopy (SEM) micrographs clearly distinguish between the surface morphology of pineapple leaf fibers treated with 5% NaOH (TPALF) and untreated fibers (UPALF). Figure 1A shows that the untreated fiber has a rough, uneven surface covered with lignin, wax, and other non-cellulosic contaminants. In composite applications, these materials produce a physical barrier that prevents efficient bonding with the polymer matrix. Furthermore, the surface is covered in voids and debris, which hinders composite constructions' capacity to transfer weight effectively. The fiber's natural composition, featuring high levels of hemicellulose, lignin, and wax, results in surface imperfections and impurities. Following NaOH treatment, the TPALF SEM image (Figure 1B) shows a striking change in surface morphology. Alkali treatment effectively removes hemicellulose and lignin, resulting in a smoother and cleaner surface.[67]

A greater specific surface area is produced by the cellulose microfibrils being more exposed and aligned. This improved surface state in composites encourages better interfacial bonding with the epoxy matrix. The absence of surface debris enhances the fiber's wettability, leading to better matrix impregnation in composite construction. The enhancement of the composites' mechanical, thermal, and tribological performance is directly attributed to these morphological modifications. Following a 5% NaOH treatment, the chemical composition analysis shows (Table 2) notable alterations in PALF. Untreated PALF's high cellulose (63.24%) level is accompanied by significant amounts of hemicellulose (14.67%), lignin (11.54%), and wax (0.74%), leading to brittleness and weak matrix adherence.

These constituents, particularly hemicellulose and lignin, are responsible for the fiber's brittleness and weak interfacial adhesion with the polymer matrix. Following treatment, the concentration of cellulose increases to 80.33%, while lignin and hemicellulose levels decrease to 6.30% and 5.72%, respectively. The removal of these non-cellulosic components improves the dimensional stability and mechanical properties of the fiber. Furthermore, the wax and moisture content decrease, which improves compatibility, dimensional stability, and water resistance. The fiber density increases from 1546 to 1587 kg/m^3 when low-density components are eliminated. These chemical modifications enhance the fiber's capacity to serve as a reinforcing material in composites. The FTIR analysis of UPALF and 5% NaOH TPALF reveals significant structural changes, as shown in Figure S4. In untreated PALF, a strong O—H peak around 3400 cm^{-1} and a C—H peak near 2900 cm^{-1} indicate the presence of hydroxyl and aliphatic groups from cellulose, hemicellulose, lignin, and wax. The peaks at 1730 cm^{-1} and 1500–1600 cm^{-1} show the C═O stretching of hemicellulose and aromatic lignin, indicating a notable amount of non-cellulosic content. The removal of the 1730 cm^{-1} peak and reduced intensity in

TABLE 2 Chemical properties of UPALF and TPALF.

Fiber type	Cellulose content (wt%)	Hemicellulose content (wt%)	Lignin content (wt%)	Wax (wt%)	Moisture content (wt%)	Ash content (wt%)	Density (kg/m^3)
UPALF	3.24 ± 1.2	14.67 ± 0.8	11.54 ± 0.6	0.74 ± 0.05	6.52 ± 0.3	3.26 ± 0.2	1546 ± 10
5% NaOH-TPALF	80.33 ± 1.1	5.72 ± 0.5	6.30 ± 0.4	0.33 ± 0.03	3.62 ± 0.2	3.67 ± 0.2	1587 ± 12

the 1500–1600 cm^{-1} range after NaOH treatment indicates successful extraction of hemicellulose and lignin. Augmented O—H stretching at 3400 cm^{-1} and distinct C—O—C peaks between 1030 and 1050 cm^{-1} signify heightened cellulose exposure. These modifications produce cleaner, denser cellulose fibers that are more hydrophilic, mechanically strong, and compatible with matrices, making TPALF better suited for composite applications.

3.2 | Field emission scanning electron microscopy characterization of alumina powder

The field emission scanning electron microscopy (FESEM) images and particle size distribution analysis provide detailed insights into the shape and size characteristics of the alumina powder. The FESEM micrograph (Figure S5a) reveals that the alumina particles are mostly spherical with smooth surfaces, demonstrating shape homogeneity. The spherical shape improves flowability and packing density, rendering the powder appropriate for use in composite manufacturing and coatings. The lack of substantial aggregation in the photograph indicates the excellent dispersibility of the alumina powder within matrices. The particle size distribution histogram (Figure S5b) shows that most particles range from 10 to 30 μm, with an average size of about 20 μm. The homogeneous particle size distribution ensures constant mechanical reinforcement and thermal characteristics when utilized as a filler in composite materials. The spherical shape and uniform size of the alumina powder improve its dispersion in epoxy or polymer matrices, enhancing the performance of the composites.

3.3 | Mechanical properties of PALF composites

The mechanical properties of the composite, such as tensile strength, flexural strength, and impact strength, significantly improved after NaOH treatment of PALF, with further enhancement from alumina fillers. The UPALF has the lowest values for tensile strength

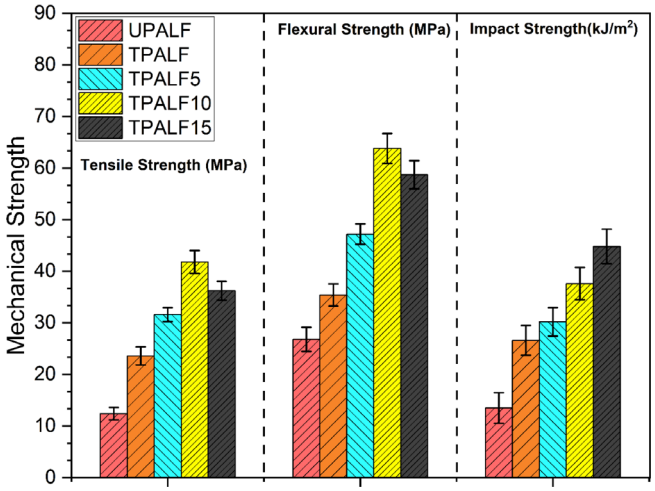

FIGURE 2 Mechanical test result.

(12.4 MPa), flexural strength (26.8 MPa), and impact strength (13.5 kJ/m^2) among all materials. The low values are due to surface impurities like lignin and wax, which hinder proper bonding with the epoxy matrix. TPALF shows marked improvements in tensile strength (23.6 MPa), flexural strength (35.4 MPa), and impact strength (26.6 kJ/m^2) because the removal of hemicellulose and lignin exposes cellulose microfibrils, enhancing fiber-matrix adhesion (Figure 2).

The addition of alumina fillers significantly enhances the mechanical properties. The TPALF5 composite has a tensile strength of 31.6 MPa, a flexural strength of 47.2 MPa, and an impact strength of 30.2 kJ/m^2, indicating that alumina particles improve load transmission and rigidity. TPALF10 offers the highest tensile strength (41.4 MPa) and flexural strength (63.8 MPa) due to its 10% alumina content, which improves stiffness and ensures better stress distribution. In TPALF15, tensile strength drops to 36.2 MPa and flexural strength to 58.7 MPa, likely due to particle agglomeration at high filler content, which causes stress concentrations and reduces load transfer efficiency. The impact strength consistently rises across all composites, with TPALF15 exhibiting the maximum value of 46.8 kJ/m^2. This enhancement is ascribed to the capacity of alumina particles to absorb energy and augment toughness. NaOH treatment and adding 10%

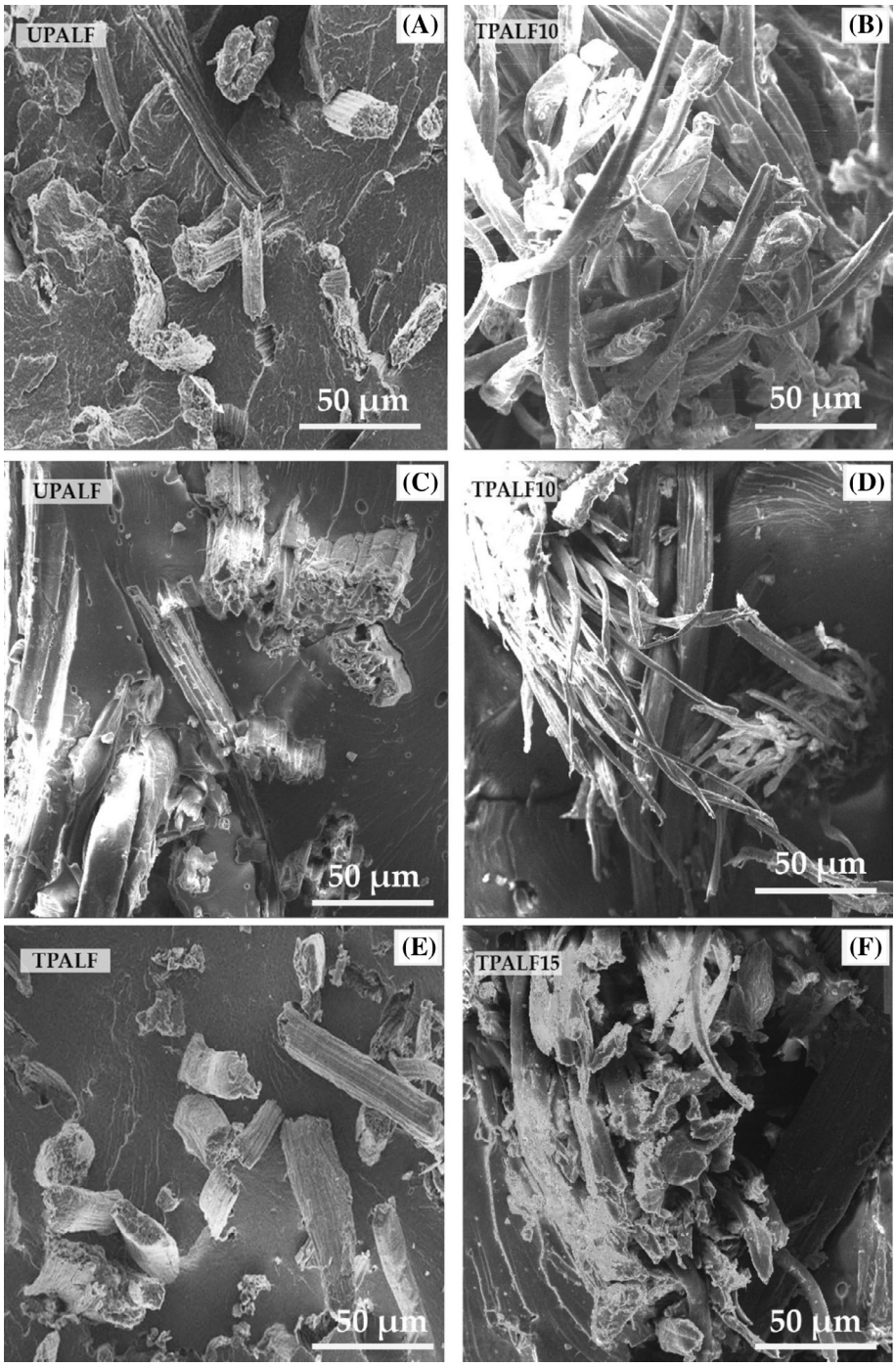

FIGURE 3 Scanning electron microscopy analysis of mechanical test fractured specimens. (A,B) Tensile test, (C,D) flexural test, and (E,F) impact test.

alumina fillers significantly enhance the mechanical properties of PALF-epoxy composites, improving tensile and flexural strength.

3.3.1 | SEM examination of fractured mechanical test specimens

The SEM analysis of cracked surfaces from tensile tests on UPALF and TPALF10 shows differences in the fiber-matrix interface and failure mechanisms, highlighting the impact of NaOH treatment and alumina filler addition. Figure 3A shows poor interfacial bonding due to significant gaps and voids around the fibers. Polished fiber surfaces show weak adhesion and fiber pullout, likely due to contaminants like wax and lignin that prevent effective stress transfer. TPALF10 (Figure 3B) shows better interfacial bonding and matrix adhesion, with minimal fiber pullout and noticeable fiber breakage. The 10% alumina concentration improves mechanical interlocking and load transfer without causing agglomeration. The data show that UPALF has weak bonding, while TPALF10 exhibits

strong adhesion and better mechanical performance due to NaOH treatment and alumina reinforcement.

The stress–strain curve (Figure S6) from the tensile test shows the mechanical properties of the composites under tensile forces. UPALF has low tensile strength and strain, showing its brittleness and poor fiber-matrix adhesion due to surface contaminants like lignin and wax. The TPALF shows improved tensile strength and strain thanks to NaOH treatment, which removes surface contaminants and enhances fiber-matrix adhesion. Composites reinforced with alumina fillers (TPALF5, TPALF10, and TPALF15) show improved tensile strength. TPALF10 strikes the best balance between strength and strain due to better stress transfer and reduced filler clumping. TPALF15 has elevated tensile strength but demonstrates somewhat decreased strain, presumably attributable to enhanced stiffness resulting from greater filler content.

Figure 3C,D illustrates the SEM examination of the cracked surfaces from the flexural test. The damaged surface of UPALF (Figure 3C) shows noticeable fiber pullout and weak adhesion between the fiber and matrix, indicated by large voids and smooth fiber surfaces. Inadequate bonding arises when surface contaminants like lignin, wax, and hemicellulose hinder efficient stress transmission during flexural loading. Insufficient adherence results in reduced flexural strength because the fibers fail to adequately reinforce the matrix. The fracture surface of TPALF10 (Figure 3D) exhibits optimal interfacial bonding, characterized by low fiber pullout and significant fiber breakage. The fibers are uniformly dispersed and securely anchored in the matrix, signifying robust mechanical interlocking and efficient stress transmission. The use of 10% alumina filler improves stiffness and load distribution, resulting in enhanced flexural performance. The matrix seems to have infiltrated the fiber structure extensively, hence enhancing the composite's strength.

The SEM examination of the fractured surfaces from the impact test for TPALF and TPALF15 elucidates the fiber-matrix interaction and failure processes under dynamic loading conditions, demonstrating the impacts of NaOH treatment and alumina filler incorporation. The broken surface of TPALF (Figure 3E) exhibits considerable fiber pullout and matrix cracking, signifying enhanced, still suboptimal fiber-matrix adhesion. The elimination of surface contaminants via NaOH treatment improves bonding, as seen by fewer voids in comparison to untreated fibers. Nevertheless, several voids surrounding the fibers indicate insufficient stress transfer during impact loading, resulting in limited energy absorption. The cracked surface of TPALF15 (Figure 3F) exhibits exceptional interfacial adhesion and energy absorption capabilities. The fibers are effectively embedded in the matrix with minimal pullout, and there is significant plastic deformation around the fibers, indicating good stress transfer and improved impact strength. The 15% alumina filler significantly augments the composite's capacity to absorb impact energy by offering further reinforcement. Nevertheless, little aggregation of filler particles may lead to localized stress concentrations, shown as tiny cracks in the matrix. The SEM examination shows that TPALF has moderate bonding, but TPALF15, treated with NaOH and with more alumina filler, exhibits better fiber-matrix interaction and energy dissipation, resulting in improved impact strength and toughness.

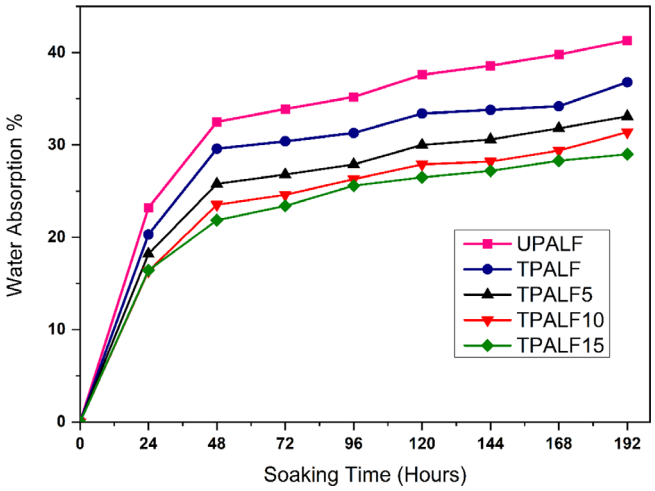

FIGURE 4 Water absorption behavior of fabricated samples.

3.4 | Water absorption behavior

The water absorption characteristics displayed by the produced samples (Figure 4) reveal a unique pattern influenced by the treatment of the fibers and the concentration of alumina filler. UPALF has the highest water absorption percentage due to its hemicellulose and lignin content, which are very hydrophilic and retain moisture. TPALF has significantly lower water absorption than UPALF because NaOH treatment removes hemicellulose and lignin, exposing hydrophobic cellulose and reducing moisture retention. The use of alumina fillers further reduces water absorption, with TPALF15 demonstrating the lowest percentage of water absorption. Alumina particles create a barrier effect, significantly reducing water intrusion into the composite.

All samples show stable water absorption over time, with composites with more alumina content displaying better moisture resistance. These findings indicate that the composites' water resistance is significantly enhanced by NaOH treatment and alumina reinforcement. Consequently, they are more suitable for use in humid environments.

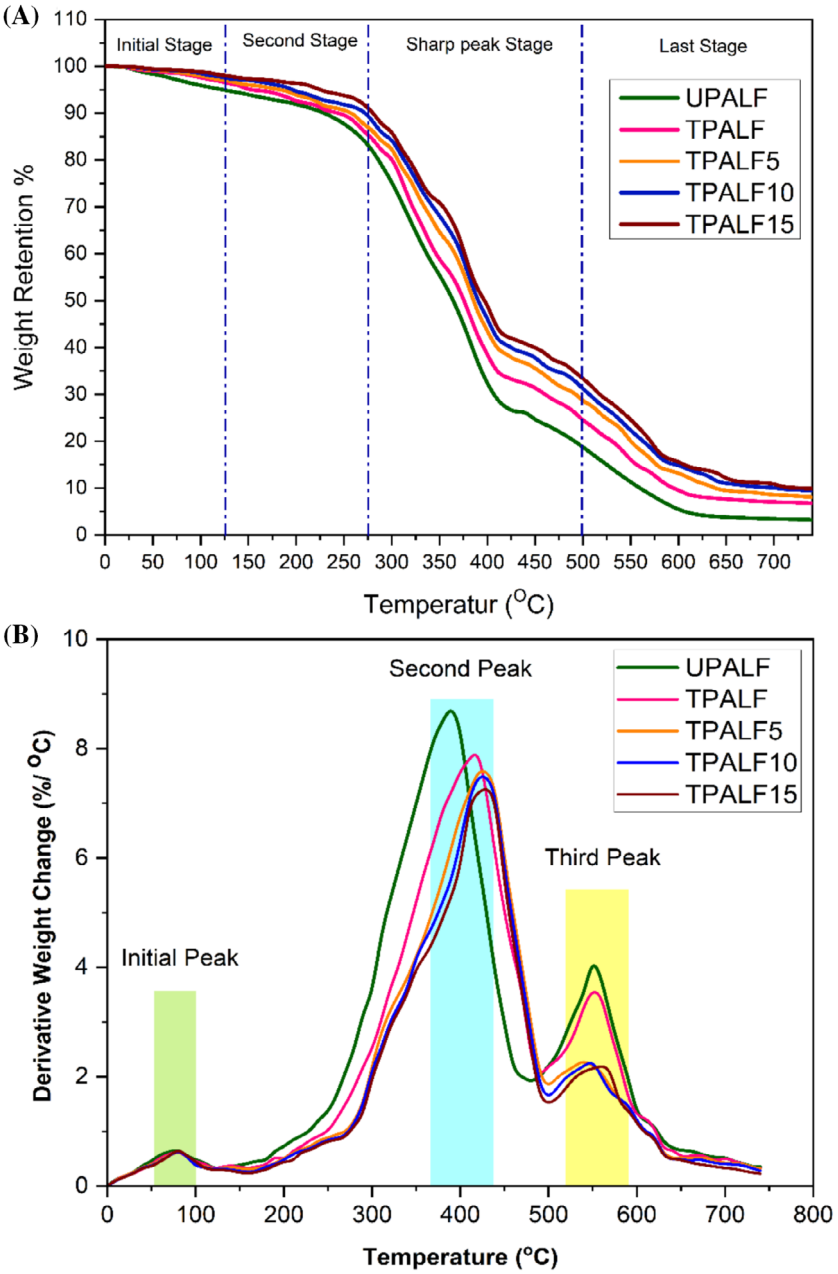

FIGURE 5 (A) Thermal degradation analysis (TGA). (B) Derivative thermogravimetry weight-loss analysis (DTG).

3.5 | Thermal degradation properties of PALF composites

The thermal degradation of the composites was studied using thermogravimetric analysis (TGA) and derivative thermogravimetry (DTG), illustrated in Figure 5. The results indicate a multi-stage decomposition process, reflecting the effects of fiber treatment and alumina reinforcement on thermal stability.

Initial Stage (50–150°C): *Moisture and volatile component evaporation*: At this stage, weight loss mainly occurs due to moisture evaporation and the release of volatile compounds. The TGA curve in Figure 5A shows that UPALF has the most weight loss because it has a higher hydrophilic content, including hemicellulose and lignin. TPALF and alumina-reinforced composites (TPALF5, TPALF10, and TPALF15) experience less weight loss, indicating that NaOH treatment decreases moisture retention, and the hydrophobic alumina fillers reduce water absorption. The DTG curve (Figure 5B) confirms this behavior, where the initial peak (~100°C) exhibits a weight change of 0.7–0.75%/°C. The peak is particularly prominent in UPALF, demonstrating a greater loss of moisture. In contrast, TPALF and alumina-filled composites exhibit lower weight changes, indicating better thermal resistance to moisture loss.

Second stage (150–300°C): *Hemicellulose decomposition and lignin degradation*: This stage corresponds to the

decomposition of hemicellulose and partial lignin breakdown. The TGA curve shows that UPALF undergoes significant weight loss, attributed to its higher hemicellulose content. However, TPALF and alumina-filled composites exhibit reduced weight loss due to hemicellulose removal via NaOH treatment and the thermal barrier effect of alumina fillers, which restrict heat penetration and delay decomposition. In the DTG plot, a sharp weight loss increase occurs around 250–300°C, with UPALF decomposing faster than the treated and alumina-reinforced composites.

Sharp peak stage (300–500°C): *Cellulose and major lignin decomposition*: This phase involves the main degradation of cellulose and the breakdown of leftover lignin, marked by a significant peak in the DTG plot (~390–428°C, Figure 5B). The TGA curve indicates that all composites undergo rapid weight loss, but TPALF10 and TPALF15 show greater thermal stability. This is due to alumina fillers, which act as heat barriers and improve thermal resistance. The DTG peak decomposition values reveal a clear trend in thermal stability among the composites. UPALF exhibits the highest decomposition rate, with an 8.8% weight change at 390°C, indicating its lower thermal resistance. TPALF has a delayed decomposition at 412°C, showing an 8.0% weight change due to the thermal stability enhancement from NaOH treatment. Adding more alumina leads to higher temperatures, as shown by TPALF5 (7.8% at 415°C), TPALF10 (7.6% at 423 C), and TPALF15 (7.3% at 428°C). Higher alumina content enhances thermal resistance, acting as a heat barrier that slows degradation and reduces decomposition rates. This makes TPALF15 the most thermally stable composite in the study.

Final stage (500–800°C): *Residual lignin and char decomposition*: At this stage, the gradual degradation of residual lignin and char occurs. The TGA curve shows that TPALF10 and TPALF15 retain more weight, indicating higher char residue formation. This suggests that alumina additives contribute to enhanced thermal stability, as they remain thermally stable at elevated temperatures. The DTG plot supports this observation, where the third peak (~600°C) represents the slow degradation of remaining lignin and char. TPALF10 and TPALF15 exhibit lower weight loss rates, further confirming their thermal resistance enhancement. TGA and DTG analyses show that treated fibers and alumina-reinforced composites are much more thermally stable than untreated samples. TPALF10 and TPALF15 have better thermal resistance due to alumina fillers that minimize heat transfer and enhance char retention. Additionally, NaOH treatment enhances thermal stability by removing hemicellulose and lignin, which are more susceptible to thermal degradation. The findings suggest that TPALF10 and TPALF15 are ideal for high-temperature use due to their better thermal resistance and lower decomposition rates.

3.6 | Sliding wear performance of PALF composites

A sliding wear test was conducted to analyze how alumina reinforcement affects the tribological behavior of TPALF5, TPALF10, and TPALF15 composites. Incorporating ANN prediction and RSM optimization, this analysis implemented both predictive and experimental modeling methodologies. To understand wear behavior and optimize operating parameters, we evaluated sliding wear performance under different conditions, such as sliding velocity, load, distance, and alumina content. Table S1 illustrates the results of the experiment.

Using experimental testing along with ANN predictive modeling provides a strong approach for analyzing and improving the tribological performance of composites. ANN was used to predict SWR and COF, while RSM optimization found the best input parameters to reduce wear and improve performance. This methodology enhances the understanding of the sliding wear behavior of alumina-reinforced composites, highlighting their suitability for wear-resistant applications. The detailed step-by-step procedure for the ANN-based Sliding Wear Test Prediction is provided in Appendix S1. The optimal number of neurons and transfer functions for the ANN analysis was determined through hyperparameter optimization with GridSearchCV. After testing various neuron values, the optimal range of 2–8 neurons was chosen as it resulted in the lowest mean squared error (MSE) and the highest R^2 accuracy in training and validation. The architecture of ANN is illustrated in Figure S7. This systematic methodology led to the development of an optimized ANN model, delivering exceptional predictive accuracy.

3.6.1 | ANN model performance

The optimized ANN models are evaluated on the validation set, generating COF predictions with the.predict() method on the validation data (X_val). The model's performance is evaluated using MSE, which calculates the average squared difference between predicted and actual values, and R^2, which shows how much variance in the target variable is explained by the model. In the first evaluation, the COF model had a MAE of 0.3479 and R^2 of 0.9634. In the second evaluation, it improved with an MAE of 0.0145 and an R^2 of 0.9725. These results demonstrate the model's high accuracy, with a near-perfect R^2 score of 0.9725, indicating excellent predictive performance.

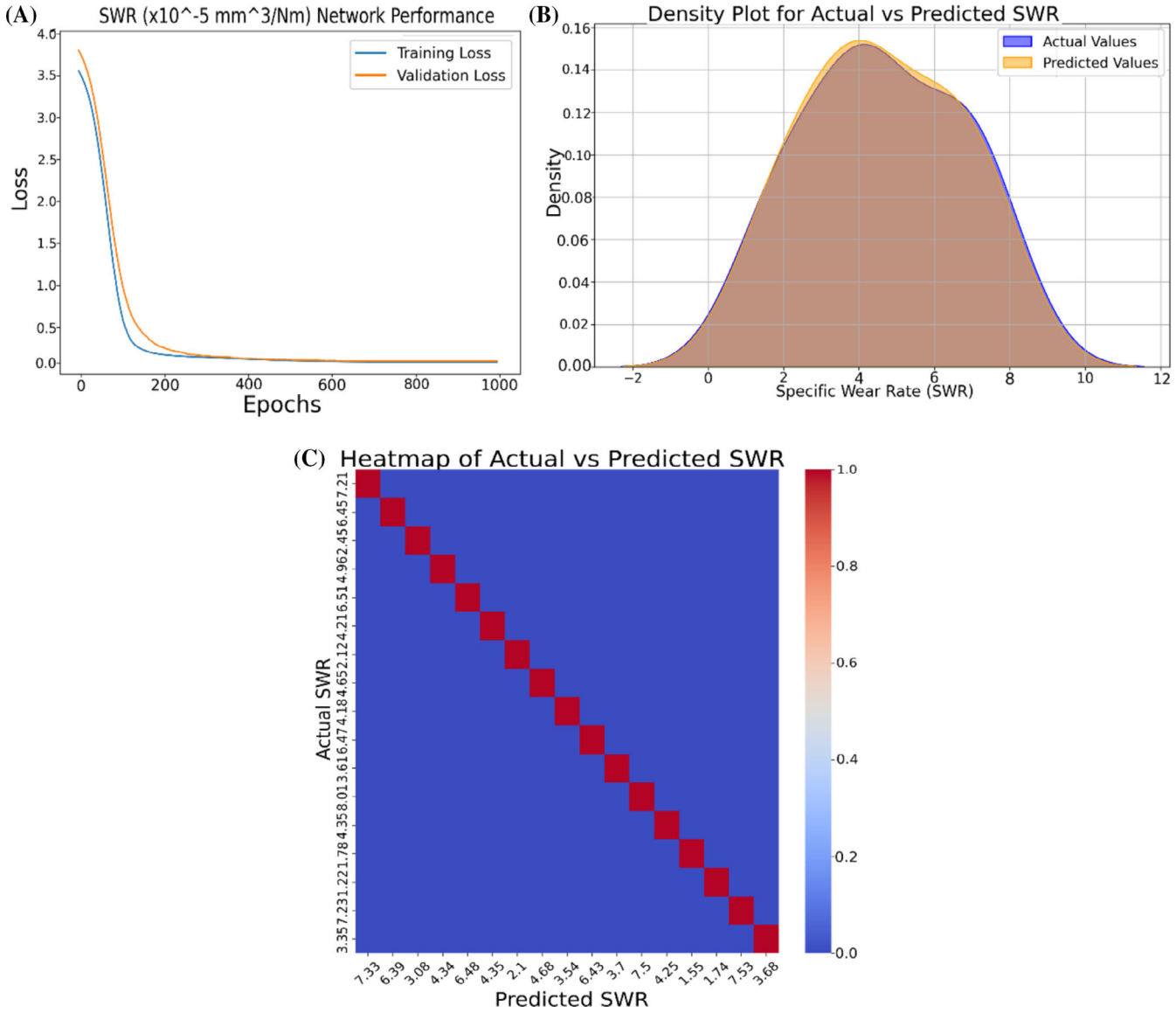

FIGURE 6 Specific wear rate (SWR) model performance. (A) Training and validation curve. (B) density plot for actual versus predicted values. (C) Heatmap of actual versus predicted values.

The low MAE and MSE values show that the ANN model accurately predicts COF under different tribological conditions, demonstrating its effectiveness in understanding the data relationships. The effectiveness of the ANN model in predicting SWR is assessed using several methods: training and validation loss curves, a density plot comparing actual and predicted SWR values, and a heatmap showing the correlation between them (Figure 6). As the number of epochs increases, the training and validation loss curves in Figure 6A steadily decrease and converge around 1000 epochs. The model reduces training errors without overfitting, as the validation loss is similar to the training loss. The ANN's ability to generalize effectively to unobserved data is illustrated by the seamless convergence.

A density diagram comparing the distribution of actual and predicted SWR values is depicted in Figure 6B. The model's high prediction accuracy is shown by the close alignment of the predicted and actual values. The alignment indicates that the model effectively captures the underlying relationship between the target variable and the input features. A heatmap of actual versus predicted SWR values is illustrated in Figure 6C. The strong diagonal pattern suggests a close match between the true values and the predictions. The high correlation and minimal error in predictions are indicated by the concentration of red along the diagonal. The results show that the ANN model is reliable and effective in predicting SWR, demonstrated by its consistent performance on various evaluation metrics.

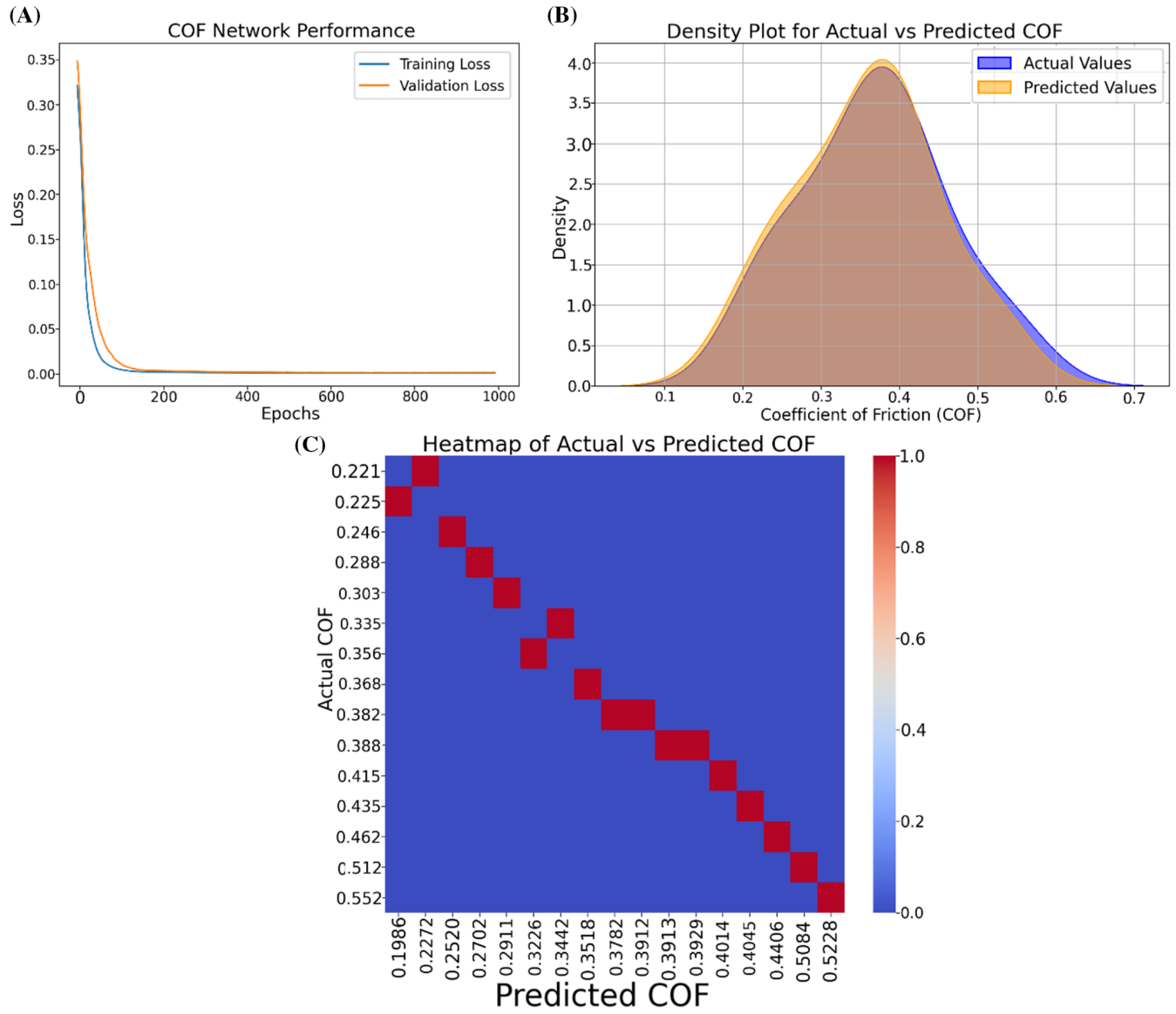

FIGURE 7 Coefficient of friction (COF) model performance. (A) Training and validation curve. (B) Density plot for actual versus predicted values. (C) Heatmap of actual versus predicted values.

The training and validation loss curves in Figure 7A steadily decrease with more epochs and level off around 1000 epochs. The validation and training loss curves are closely aligned, indicating that the model effectively reduces prediction error and avoids overfitting. This clearly illustrates that the ANN model has successfully adapted to previously unseen data. Figure 7B shows a density diagram indicating that the predicted COF values closely match the actual values. The model's high predictive accuracy is shown by the alignment of actual and predicted distributions, demonstrating the relationship between input features and the target variable. A heatmap of actual versus predicted COF values is depicted in Figure 7C. The model's precision is highlighted by the strong diagonal alignment, showing a great match between actual and predicted COF values. There is a strong correlation between actual and predicted outputs, shown by the red areas along the diagonal, indicating low prediction error. The ANN model performs well in predicting COF, as shown by a strong heatmap correlation, closely aligned actual and predicted distributions, and low loss values. This guarantees the model's robustness and dependability in accurately predicting tribological behavior under a variety of operating conditions.

3.6.2 | Cross-validation of ANN

The learning curves presented in Figure 8 illustrate the model performance for predicting SWR and COF using Machine Learning. The MSE is plotted against the

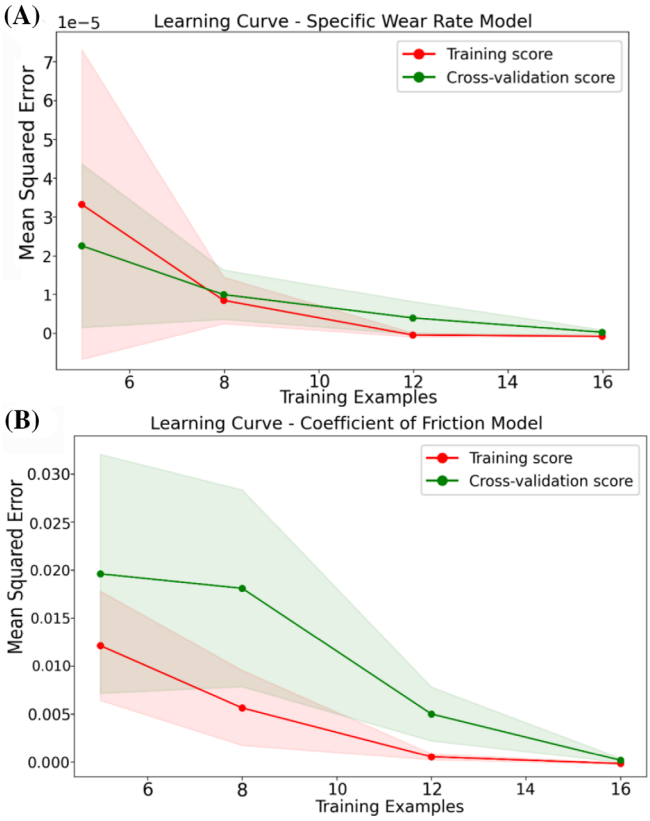

FIGURE 8 Cross-validation for (A) specific wear rate (SWR) and (B) coefficient of friction (COF) models.

number of training examples, with separate curves for training score (red) and cross-validation score (green). The shaded regions indicate variability in error across different folds in cross-validation.

In Figure 8A, the SWR model initially exhibits a high MSE for both training and cross-validation scores when trained with fewer data points. As more training examples are added, the error reduces, and both curves converge, indicating improved model generalization. The narrow gap between the two curves at the right end suggests that the model has learned effectively from the data, minimizing overfitting and achieving stable predictions. Similarly, in Figure 8B, the COF model follows a comparable trend. The training score starts lower than the cross-validation score, signifying that the model initially performs better on the training data than on unseen data. However, as the training size increases, both curves approach a lower MSE, indicating enhanced predictive accuracy. The slight difference in scores at smaller training sizes suggests minor overfitting, which diminishes with more training examples. Overall, both models demonstrate good learning behavior, as the reduction in MSE with increasing training data highlights improved generalization. The convergence of training and validation curves confirms that the models are neither underfitting nor overfitting, making them reliable for predicting SWR and COF in tribological analysis.

3.6.3 | Optimization by response surface methodology

Response surface methodology was used with Design Expert v13 to optimize the sliding wear behavior of epoxy composites reinforced with PALF and alumina filler. The tribological performance was evaluated by finding a design that considered sliding velocity, normal load, sliding distance, and alumina infill percentage. The response variables, SWR and COF, perfectly matched a quadratic model, showing an excellent fit. The quadratic model effectively represented the relationship between input parameters and responses, enabling accurate predictions and optimization. This method offers valuable insights for improving the frictional performance and wear resistance of the composites.

Analysis of variance

The analysis of variance (ANOVA) table (Table S2) for the SWR model shows the significance of input parameters and their contributions to the response. The quadratic model is robust, shown by an F-value of 169 and a p value of less than 0.0001 for the overall model of SWR. The infill percentage (D) is the most significant factor affecting SWR, explaining 93% of its variability, based on a large sum of squares and a very significant p value (<0.0001). Load (B) is statistically significant but has a minimal contribution, whereas sliding velocity (A) and sliding distance (C) are significant, contributing 4% and 2%, respectively. Sliding distance and infill percentage have non-linear effects that require careful optimization, shown by the significant interaction terms $A*D$ and the quadratic terms C^2 and D^2. The model's ability to predict SWR is demonstrated by a R^2 high of 0.9729, an adjusted R^2 of 0.9671, and a sufficient precision of 41.7623.

The ANOVA table confirms the validity of the quadratic model for the COF model, showing an F value of 956.7 and a p value under 0.0001. The infill percentage (D) remains the most significant factor, accounting for 88% of the variation in COF. Both sliding velocity (A) and sliding distance (C) have demonstrated statistically significant contributions of 9% and 2%, respectively. Although statistically significant, load (B) makes a negligible contribution. The interaction term BD and the quadratic terms A^2, B^2, and C^2 highlight the complex relationships between the parameters. The model's predictive accuracy and robustness are illustrated by its high R^2 (0.9951), amended R^2 (0.9941), and sufficient precision (106.675). The findings of this study suggest that the filler percentage is a critical

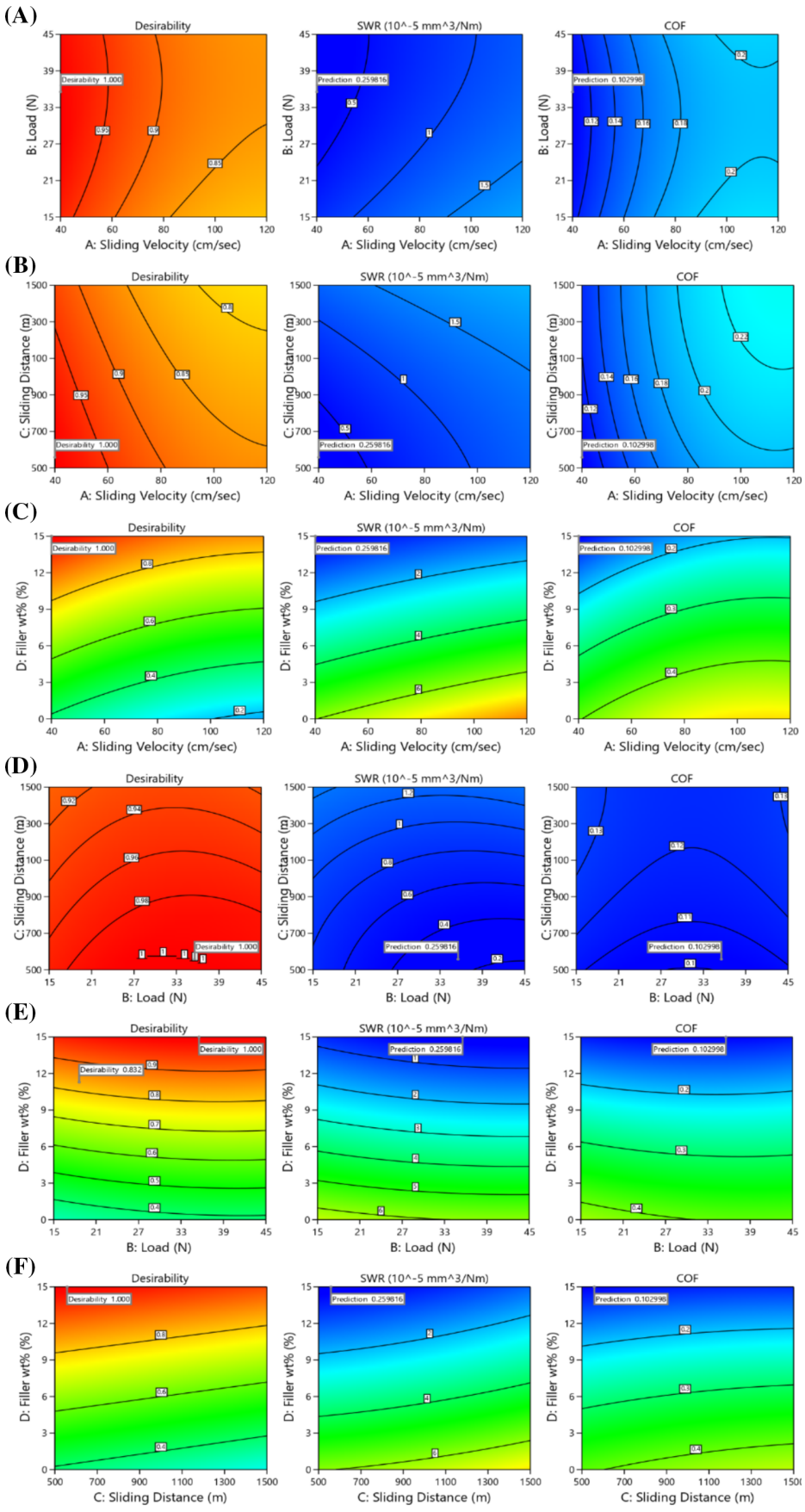

FIGURE 9 Contour interaction plot for specific wear rate (SWR) and coefficient of friction (COF) (A) A–B, (B) A–C, (C) A–D, (D) B–C, (E) B–D, and (F) C–D.

factor in both SWR and COF models. Moreover, while sliding velocity and distance do exert a significant influence, their impact is comparatively less. Consequently, the necessity for precision optimization to improve the tribological performance of the composites is demonstrated.

Contour plots for tribological behavior of PALF composites

Figure 9 presents contour interaction plots illustrating the combined effects of input parameters sliding velocity (*A*), load (*B*), sliding distance (*C*), and filler percentage (*D*) on SWR and COF. The desirability plots indicate the optimal parameter conditions for minimizing wear and friction. Figure 9A depicts the interaction between *A* and *B*. As load increases, COF shows an upward trend, while moderate sliding velocities help optimize tribological performance. At high sliding velocities, increased frictional heat causes a slight rise in SWR, but alumina reinforcement mitigates wear. Figure 9B illustrates the effect of *A* and *C*. SWR increases slightly with higher sliding distances due to greater material removal, while COF remains stable at lower sliding velocities but rises at higher velocities. In Figure 9C, the interaction between *A* and *D* is shown. Higher filler content significantly reduces both SWR and COF, demonstrating improved wear resistance and lubrication. However, excessive sliding velocity results in a moderate increase in SWR due to thermal softening effects. Figure 9D examines the influence of *B* and *C*. At higher loads and sliding distances, SWR increases due to greater surface contact stress and material loss, while COF exhibits a nonlinear trend, with intermediate values occurring at moderate load levels.

Figure 9E highlights the interaction between *B* and *D*, showing that higher filler content leads to lower SWR and COF. The lowest friction and wear values are observed at an optimal load range, reinforcing the effectiveness of alumina particles in reducing surface degradation. Finally, Figure 9F explores the relationship between *C* and *D*. Increasing sliding distance results in a gradual increase in SWR and COF, but higher filler content counteracts this effect, leading to improved tribological performance. Overall, these contour plots emphasize the importance of optimizing sliding velocity, load, and filler percentage to achieve superior wear resistance. The desirability graphs indicate that the best results are obtained at moderate sliding velocities, optimal loads, and higher filler percentages, confirming the crucial role of alumina reinforcement in PALF composites.

Optimization of input parameters

This desirability diagram (Figure S8) illustrates the optimization of input parameters to reduce the SWR and COF. The chosen parameters effectively minimize both SWR and COF, as shown by the optimal solution's desirability value of 1.000. The gliding velocity is optimized to 40.04 cm/s, guaranteeing controlled frictional heating and attrition. The sliding load is optimized at 35.55 N to achieve adequate contact stress while minimizing material removal. The sliding distance has been established at 558.13 m to mitigate attrition during extended testing. The optimal filler percentage is 15 wt%, highlighting how alumina significantly improves abrasion resistance and reduces the COF. The SWR is decreased to 0.2598×10^{-5} mm^3/Nm, and the COF is lowered to 0.103, indicating outstanding tribological performance. This optimization highlights the importance of filler content and sliding parameters in enhancing wear resistance and reducing friction in the composite.

3.6.4 | Validation of ANN and RSM with experimental value

The sliding wear test results are compared to the predicted values of SWR and COF from the ANN and RSM models in Table S3. In most test cases, the ANN model shows a lower percentage error than the RSM for SWR, averaging 0.94%. This demonstrates an improvement in prediction accuracy. The RSM model has a higher average percentage error of −1.0905%, with some errors exceeding 20%, particularly under high sliding load and velocity conditions. This underscores the model's limitations in capturing nonlinear interactions. Both the ANN model and the RSM model demonstrate remarkable predictive accuracy for COF. The ANN model has an average error of 1.08%, while the RSM model has a lower average error of 0.54%. ANN can handle complex relationships between input parameters, allowing it to perform better in certain situations, like with large sliding distances.[63,68] The table shows that the ANN model is more accurate for SWR and matches the RSM for COF, with both models providing reliable predictions. This underscores the robustness and appropriateness of ANNs for capturing the intricate and nonlinear tribological behavior of composites.

3.6.5 | SEM examination of worn surfaces

Composites with 5%, 10%, and 15% alumina filler show different wear patterns under extreme conditions (120 cm/s speed, 45 N load, and 1500 m distance) in SEM analysis of their worn surfaces. The 5% alumina sample (Figure 10A) shows a worn surface with deep fissures, pits, and significant surface degradation, indicating considerable material loss. The lack of adequate infill content does not provide enough support, leading to significant wear and damage under high sliding loads and speeds.

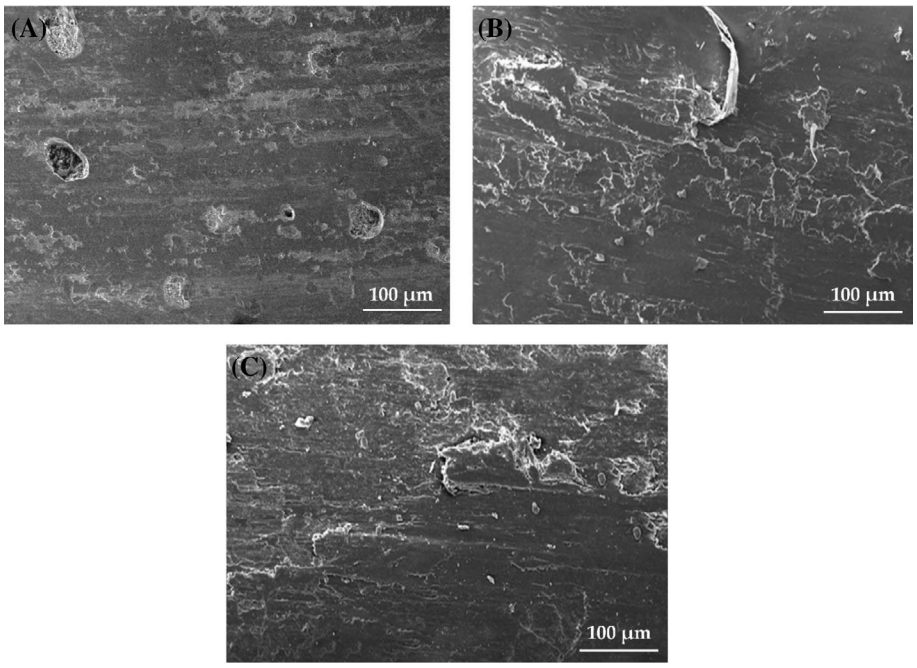

FIGURE 10 Worn surface scanning electron microscopy analysis at maximum wear condition (A) TPALF5, (B) TPALF10, and (C) TPALF15.

Poor wear resistance is the consequence of the absence of filler-induced fortification.[69]

The 10% alumina sample shows (Figure 10B) less wear than the 5% sample, featuring shallower grooves and smaller pits. The increased alumina content enhances the composite's hardness and wear resistance, mitigating the abrasive wear mechanism.[70] Localized delamination and microcracks indicate a shift to adhesive wear because of better interfacial bonding. The 15% alumina sample (Figure 10C) exhibits the least surface damage, with minimal grooves and a smoother worn surface.[71] Increased filler content delivers exceptional reinforcement, allowing the material to withstand extreme conditions without losing integrity. The alumina particles act as a barrier, reducing direct matrix-fiber interaction and distributing the load more uniformly. This results in enhanced wear resistance, with the wear mechanism dominated by mild adhesive wear and particle-induced load transfer. The analysis shows that alumina reinforcement is essential for enhancing the wear resistance of composites, with 15% alumina providing the best performance under tough conditions.

4 | CONCLUSIONS

This study evaluated the effect of NaOH treatment and alumina reinforcement on the mechanical, water absorption, thermal, and sliding wear properties of PALF-reinforced epoxy composites. NaOH treatment significantly improved fiber-matrix adhesion, enhancing tensile, flexural, and impact strength, while alumina fillers further strengthened the composites, with 10 wt% alumina providing the best balance of strength and toughness.

Water absorption tests confirmed reduced moisture uptake due to hemicellulose removal, with 15 wt% alumina composites exhibiting the lowest water absorption, ensuring durability in humid conditions. Thermal stability was enhanced, with higher char residue and decomposition temperatures observed in 15 wt% alumina composites, making them suitable for high-temperature applications. Sliding wear performance improved, with 15 wt% alumina composites achieving the lowest SWR and COF due to their hard, wear-resistant nature. SEM analysis confirmed a transition from severe abrasive wear in untreated composites to mild adhesive wear in alumina-reinforced composites.

The findings demonstrate that NaOH-treated, alumina-filled PALF composites offer enhanced mechanical strength, water resistance, thermal stability, and tribological performance, making them ideal for applications in the automotive, aerospace, and structural industries. The study highlights their potential as sustainable, high-performance bio-based composites for industrial use.

AUTHOR CONTRIBUTIONS

V. S. Shaisundaram: mechanical testing. **Saravanakumar Sengottaiyan**: research, methodology, writing draft. **Rajesh Mohan**: fabrication and experiment work. **Vishnupriya Gurunathan**: developed a Python code for ANN.

CONFLICT OF INTEREST STATEMENT

The authors no conflict of interest.

DATA AVAILABILITY STATEMENT

The data included in the supporting information file are openly accessible via DOI. The Python code for the artificial neural network (ANN) model is available upon request.

ORCID

Saravanakumar Sengottaiyan https://orcid.org/0000-0001-6655-0011

REFERENCES

1. Mishra T, Mandal P, Rout AK, Sahoo D. A state-of-the-art review on potential applications of natural fiber-reinforced polymer composite filled with inorganic nanoparticle. *Compos Part C: Open Access*. 2022;9:100298. doi:10.1016/j.jcomc.2022.100298
2. Khatri H, Naveen J, Jawaid M, Jayakrishna K, Norrrahim MNF, Rashedi A. Potential of natural fiber based polymeric composites for cleaner automotive component production—a comprehensive review. *J Mater Res Technol*. 2023;25:1086-1104. doi:10.1016/j.jmrt.2023.06.019
3. Tesfie N, BA L, Absi R, El Abbassi I. Assessment of the thermal and mechanical properties of bio-based composite materials for thermal insulation: a review. *J Build Eng*. 2024;97:110605. doi:10.1016/j.jobe.2024.110605
4. Karthik K, Rajamanikkam R k, Venkatesan EP, et al. State of the art: natural fibre-reinforced composites in advanced development and their physical/chemical/mechanical properties. *Chin J Anal Chem*. 2024;52(7):100415. doi:10.1016/j.cjac.2024.100415
5. Saba N, Jawaid M. A review on thermomechanical properties of polymers and fibers reinforced polymer composites. *J Ind Eng Chem*. 2018;67:1-11. doi:10.1016/j.jiec.2018.06.018
6. Elfaleh I, Abbassi F, Habibi M, et al. A comprehensive review of natural fibers and their composites: an eco-friendly alternative to conventional materials. *Results Eng*. 2023;19:101271.
7. Muthalagu R, Sathees Kumar S, Pati PR, Giri J, Sathish T, Fatehmulla A. Influence of Prosopis juliflora bark powder/fillers on the mechanical, thermal and damping properties of jute fabric hybrid composites. *J Mater Res Technol*. 2024;33:3452-3461. doi:10.1016/j.jmrt.2024.10.066
8. Keerthiveettil Ramakrishnan S, Vijayananth K, Pudhupalayam Muthukutti G, Spatenka P, Arivendan A, Ganesan SP. The effect of various composite and operating parameters in wear properties of epoxy-based natural fiber composites. *J Mater Cycles Waste Manag*. 2022;24:667-679. doi:10.1007/s10163-022-01357-1
9. Neto J, Queiroz H, Aguiar R, Lima R, Cavalcanti D, Banea MD. A review of recent advances in hybrid natural fiber reinforced polymer composites. *J Renew Mater*. 2022;10:561-589. doi:10.32604/jrm.2022.017434
10. Paknejad R, Ghasemi FA, Fard KM. Analysis of free vibration and low-velocity impact response on Sandwich cylindrical shells containing fluid. *Mech Compos Mater*. 2024;60:729-750. doi:10.1007/s11029-024-10223-0
11. Kumar SS, Shyamala P, Pati PR, Gandla PK. Wear and frictional performance of epoxy composites reinforced with natural waste fibers and fillers for engineering applications. *Fibers Polym*. 2024;25:1429-1442. doi:10.1007/s12221-024-00519-2
12. Bolduc S, Jung K, Venkata P, et al. Banana fiber/low-density polyethylene recycled composites for third world eco-friendly construction applications—waste for life project Sri Lanka. *J Reinf Plast Compos*. 2018;37:1322-1331. doi:10.1177/0731684418791756
13. Vinod B, Anandajothi M. Mechanical and tribological properties of abaca-roselle/cardanol formaldehyde hybrid composites. *Mater Res Express*. 2020;6(12):125363. doi:10.1088/2053-1591/ab66fa
14. Raj SSR, Dhas JER, Jesuthanam CP. Challenges on machining characteristics of natural fiber-reinforced composites—a review. *J Reinf Plast Compos*. 2021;40:41-69. doi:10.1177/0731684420940773
15. Kavya HM, Bavan S, Yogesha B, Sanjay MR, Siengchin S, Gorbatyuk S. Effect of coir fiber and inorganic filler on physical and mechanical properties of epoxy based hybrid composites. *Polym Compos*. 2021;42:3911-3921. doi:10.1002/pc.26103
16. Chougala V, Gowda AC, Nagaraja S, Imam M. Effect of chemical treatments on mechanical properties of sugarcane bagasse (Gramineae *Saccharum officinarum* L.) fiber based biocomposites: a review. *J Nat Fibers*. 2025;22(1):2445571. doi:10.1080/15440478.2024.2445571
17. Umashankaran M, Gopalakrishnan S. Effect of sodium hydroxide treatment on physico-chemical, thermal, tensile and surface morphological properties of *Pongamia pinnata* L. bark fiber. *J Nat Fibers*. 2021;18:2063-2076. doi:10.1080/15440478.2019.1711287
18. Pradhan P, Purohit A, Singh J, et al. Tribo-performance analysis of an agro-waste-filled epoxy composites using finite element method. *J Inst Eng Ser E*. 2022;103(2):339-345. doi:10.1007/s40034-022-00243-7
19. Purohit A, Pradhan P, Palanimuthu S, Kumar A, Chauhan PK. Mechanical and tribological characteristics of glass fiber and rice stubble-filled epoxy-LD sludge hybrid composites. *J Elast Plast*. 2024;57:113-131. doi:10.1177/00952443241305709
20. Purohit A, Dehury J, Sitani A, et al. A novel study on the stacking sequence and mechanical properties of jute-Kevlar-epoxy composites. *Interactions*. 2024;245:100. doi:10.1007/s10751-024-01946-6
21. Das C, Mishra SK, Purohit A. Evaluation of surface response of *Ficus benghalensis* fiber—epoxy composites under dry sliding Wear conditions. *J Inst Eng Ser E*. 2022;103:47-52. doi:10.1007/s40034-020-00182-1
22. Purohit A, Dehury J, Rout LN, Pal S. A novel study of synthesis, characterization and erosion Wear analysis of glass–jute polyester hybrid composite. *J Inst Eng Ser E*. 2023;104:1-9. doi:10.1007/s40034-023-00268-6
23. Dash S, Satpathy MP, Routara BC, Pati PR, Gantayat S. Enhancing mechanical and tribological performance of hybrid composites: an experimental study utilizing response surface methodology and firefly algorithm. *Polym Compos*. 2024;45:15924-15940. doi:10.1002/pc.28880
24. Kumar SS, Shyamala P, Pati PR, Giri J, Makki E, Sathish T. Mechanical (static and dynamic) characterization and thermal stability of hybrid green composites for engineering applications. *J Mater Res Technol*. 2024;30:7214-7227. doi:10.1016/j.jmrt.2024.05.132
25. Bhowmik S, Kumar S, Mahakur VK. Various factors affecting the fatigue performance of natural fiber-reinforced polymer composites: a systematic review. *Iran Polym J*. 2024;33:249-271. doi:10.1007/s13726-023-01243-z

26. Haryati A, Razali N, Petrů M, Taha M, Muhammad N, Ilyas RA. Effect of chemically treated kenaf fibre on mechanical and thermal properties of PLA composites prepared through fused deposition modeling (FDM). *Polymers*. 2021;13(19):3299. doi:10.3390/polym13193299
27. Fiore V, Di Bella G, Valenza A. The effect of alkaline treatment on mechanical properties of kenaf fibers and their epoxy composites. *Compos Part B: Eng*. 2015;68:14-21. doi:10.1016/j.compositesb.2014.08.025
28. Gunge A, Koppad PG, Nagamadhu M, Kivade SB, Murthy KVS. Study on mechanical properties of alkali treated plain woven banana fabric reinforced biodegradable composites. *Compos Commun*. 2019;13:47-51. doi:10.1016/j.coco.2019.02.006
29. Vilay V, Mariatti M, Mat Taib R, Todo M. Effect of fiber surface treatment and fiber loading on the properties of bagasse fiber-reinforced unsaturated polyester composites. *Compos Sci Technol*. 2008;68:631-638. doi:10.1016/j.compscitech.2007.10.005
30. Sathiyamurthy S, Saravanakumar S, Ananthi N, Devi P. Optimization of fiber length and filler content for improving the mechanical behaviour of musa acuminate fiber-reinforced epoxy composite using response surface methodology. *J Ceram Process Res*. 2023;24:683-692. doi:10.36410/jcpr.2023.24.4.683
31. Aredla R, Dasari HC, Kumar SS, Pati PR. Mechanical properties of natural fiber reinforced natural and ceramic fillers for various engineering applications. *Interactions*. 2024;245:249. doi:10.1007/s10751-024-02109-3
32. Velmurugan G, Siva Shankar V, Natrayan L, et al. Multiresponse optimization of mechanical and physical adsorption properties of activated natural fibers hybrid composites. *Adsorpt Sci Technol*. 2022;2022:1384738. doi:10.1155/2022/1384738
33. Sumesh KR, Kanthavel K. Synergy of fiber content, Al_2O_3 nanopowder, NaOH treatment and compression pressure on free vibration and damping behavior of natural hybrid-based epoxy composites. *Polym Bull*. 2020;77:1581-1604. doi:10.1007/s00289-019-02823-x
34. Vinay SS, Sanjay MR, Siengchin S, Venkatesh CV. Effect of Al_2O_3 nanofillers in basalt/epoxy composites: mechanical and tribological properties. *Polym Compos*. 2021;42:1727-1740. doi:10.1002/pc.25927
35. Todkar SS, Patil SA. Review on mechanical properties evaluation of pineapple leaf fibre (PALF) reinforced polymer composites. *Compos Part B: Eng*. 2019;174:106927. doi:10.1016/j.compositesb.2019.106927
36. Deeban B, Maniraj J, Ramesh M. Experimental investigation of properties and aging behavior of pineapple and sisal leaf hybrid fiber-reinforced polymer composites. *E-Polymers*. 2023;23:8104. doi:10.1515/epoly-2022-8104
37. Jain J, Sinha S. Pineapple leaf fiber polymer composites as a promising tool for sustainable, eco-friendly composite material: review. *J Nat Fibers*. 2022;19:10031-10052. doi:10.1080/15440478.2021.1993478
38. Cisneros-López EO, González-López ME, Pérez-Fonseca AA, González-Núñez R, Rodrigue D, Robledo-Ortíz JR. Effect of fiber content and surface treatment on the mechanical properties of natural fiber composites produced by rotomolding. *Compos Interfaces*. 2017;24:35-53. doi:10.1080/09276440.2016.1184556
39. Asri RIS, Sunendar B, Dwiandhono I, Harmaji A. Properties of metal oxide and pineapple fiber reinforced dental composite resin. *Phys Chem Solid State*. 2023;24:692-698. doi:10.15330/pcss.24.4.692-698
40. Hoque MB, Hannan MA, Mollah MZI, Faruque MRI, Khan RA. Physico-mechanical properties enhancement of pineapple leaf fiber (PALF) reinforced epoxy resin-based composites using guar gum (polysaccharide) filler: effects of gamma radiation. *Radiat Eff Defects Solids*. 2022;177:401-416. doi:10.1080/10420150.2022.2043317
41. Aynalem GF, Sirahbizu B. Effect of Al_2O_3 on the tensile and impact strength of flax/unsaturated polyester composite with emphasis on automobile body applications. *Adv Mater Sci Eng*. 2021;2021(1):6641029. doi:10.1155/2021/6641029
42. Swain PTR, Biswas S. Influence of fiber surface treatments on physico-mechanical behaviour of jute/epoxy composites impregnated with aluminium oxide filler. *J Compos Mater*. 2017;51:3909-3922. doi:10.1177/0021998317695420
43. Saha A, Kumar S, Kumar A. Influence of pineapple leaf particulate on mechanical, thermal and biodegradation characteristics of pineapple leaf fiber reinforced polymer composite. *J Polym Res*. 2021;28(2):66. doi:10.1007/s10965-021-02435-y
44. Praveena B, Shettty BP, Sachin B, Yadav SPS, Avinash L. Physical and mechanical properties, morphological behaviour of pineapple leaf fibre reinforced polyester resin composites. *Adv Mater Process Technol*. 2022;8:1147-1159. doi:10.1080/2374068X.2020.1853498
45. Gnanasekaran S, Nordin NIA A, Hamidi MMM, Shariffuddin JH. Effect of alkaline treatment on the characteristics of pineapple leaves fibre and PALF/PP biocomposite. *J Mech Eng Sci*. 2021;15:8518-8528. doi:10.15282/jmes.15.4.2021.05.0671
46. Senthilkumar K, Rajini N, Saba N, Chandrasekar M, Jawaid M, Siengchin S. Effect of alkali treatment on mechanical and morphological properties of pineapple leaf fibre/polyester composites. *J Polym Environ*. 2019;27:1191-1201. doi:10.1007/s10924-019-01418-x
47. Rajeshkumar G. Effect of sodium hydroxide treatment on dry sliding wear behavior of Phoenix sp. fiber reinforced polymer composites. *J Ind Text*. 2022;51:2819S-2834S. doi:10.1177/1528083720918948
48. Nagaraja S, Anand PB, Shivakumar HD, Ammarullah MI. Influence of fly ash filler on the mechanical properties and water absorption behaviour of epoxy polymer composites reinforced with pineapple leaf fibre for biomedical applications. *RSC Adv*. 2024;14:14680-14696. doi:10.1039/d4ra00529e
49. Sabarinathan P, Annamalai VE, Rajkumar K, Vishal K. Effects of recovered brown alumina filler loading on mechanical, hygrothermal and thermal properties of glass fiber–reinforced epoxy polymer composite. *Polym Polym Compos*. 2021;29:S1092-S10102. doi:10.1177/09673911211046780
50. Vinoth V, Sathiyamurthy S, Saravanakumar S, Senthilkumar R. Integrating response surface methodology and machine learning for analyzing the unconventional machining properties of hybrid fiber-reinforced composites. *Polym Compos*. 2024;45:6077-6092. doi:10.1002/pc.28180
51. Sathiyamurthy S, Vinoth V, Saravanakumar S, Devi P. Investigation on mechanical behaviour of calcium carbonate and groundnut shell filler added Cocos Nucifera Fiber reinforced polyester composites. *ARPN J Eng Appl Sci*. 2023;18:1425-1432. doi:10.59018/0623180

52. Saravanakumar S, Sathiyamurthy S, Pathmanaban P, Devi P. Integrating machine learning and response surface methodology for analyzing anisotropic mechanical properties of biocomposites. *Compos Interfaces*. 2024;31:1-28. doi:10.1080/09276440.2023.2260239
53. Ramesh G, Subramanian K, Sathiyamurthy S, Prakash M. *Calotropis gigantea* fiber-epoxy composites: influence of fiber orientation on mechanical properties and thermal behavior. *J Nat Fibers*. 2020;19(10):1-13. doi:10.1080/15440478.2020.1848718
54. Saravanakumar S, Sathiyamurthy S, Vinoth V, Devi P. Effect of alumina on epoxy composites with Banana fiber: mechanical, water resistance and degradation property analysis. *Fibers Polym*. 2024;25:275-287. doi:10.1007/s12221-023-00405-3
55. Periyappillai G, Sathiyamurthy S, Saravanakumar S. Optimized machine learning prediction and RSM optimization of mechanical properties in boiled eggshell filler-added biocomposites. *Fibers Polym*. 2024;25:3115-3133. doi:10.1007/s12221-024-00638-w
56. Sengottaiyan S, Sathiyamurthy S, Selvakumar G. Influence of treatment and fly ash fillers on the mechanical and tribological properties of banana fiber epoxy composites : experimental and ANN-RSM modeling. *Compos Interfaces*. 2025;1-33. doi:10.1080/09276440.2024.2448879
57. Jayabal S, Rajamuneeswaran S, Ramprasath R, Balaji NS. Artificial neural network modeling of mechanical properties of calcium carbonate impregnated coir-polyester composites. *Trans Indian Inst Metals*. 2013;66:247-255. doi:10.1007/s12666-013-0255-9
58. Sathiyamurthy S, Saravanakumar S, Vinoth V. Enhancing tribological performance of hybrid fiber-reinforced composites through machine learning and response surface methodology. *J Reinf Plast Compos*. 2024. doi:10.1177/07316844241256421
59. Sengottaiyan S, Subbarayan S, Viswanathan V, Pugazhendi P. Optimized machine learning with hyperparameter tuning and response surface methodology for predicting tribological performance in bio-composite materials. *Polym Compos*. 2024;45:9421-9439. doi:10.1002/pc.28418
60. Talib AAA, Jumahat A, Jawaid M, Sapiai N, Leao AL. Effect of wear conditions, parameters and sliding motions on tribological characteristics of basalt and glass fibre reinforced epoxy composites. *Materials*. 2021;14:1-18. doi:10.3390/ma14030701
61. Sengottaiyan S, Subbarayan S, Natarajan R, Gurunathan V. Enhancing mechanical, degradation, and tribological properties of biocomposites via treatment and alumina content. *J Reinf Plast Compos*. 2025;7316844251321664. doi:10.1177/07316844251321664
62. Saravanakumar S, Sathiyamurthy S, Vinoth V. Enhancing machining accuracy of banana fiber-reinforced composites with ensemble machine learning. *Meas J Int Meas Confed*. 2024;235:114912. doi:10.1016/j.measurement.2024.114912
63. Periyappillai G, Subbarayan S, Sengottaiyan S. Advanced ensemble machine learning prediction to enhance the accuracy of abrasive waterjet machining for biocomposites. *Mater Chem Phys*. 2025;333:130175. doi:10.1016/j.matchemphys.2024.130175
64. Saravanakumar S, Sathiyamurthy S, Ananthi N, Devi P. Optimization of drilling characteristics of Al_2O_3 and boiled eggshell filler-added hybrid bio composite from agriculture residue. *Biomass Convers Biorefinery*. 2024;14:29321-29335. doi:10.1007/s13399-023-04572-4
65. Purohit A, Satapathy A, Swain PTR. Analysis of erosion Wear behavior of LD sludge filled polypropylene composites using RSM. *Mater Sci Forum*. 2020;978:222-228. doi:10.4028/www.scientific.net/MSF.978.222
66. Murali B, Ramnath BMV, Rajamani D, Nasr EA, Astarita A, Mohamed H. Experimental investigations on dry sliding Wear behavior of Kevlar and natural fiber-reinforced hybrid composites through an RSM–GRA hybrid approach. *Materials*. 2022;15(3):749. doi:10.3390/ma15030749
67. Asim M, Jawaid M, Abdan K, Ishak MR. Effect of alkali and silane treatments on mechanical and fibre-matrix bond strength of kenaf and pineapple leaf Fibres. *J Bionic Eng*. 2016;13:426-435. doi:10.1016/S1672-6529(16)60315-3
68. Purohit A, Satapathy A. Epoxy matrix composites filled with micro-sized LD sludge: wear characterization and analysis. *IOP Conf Ser Mater Sci Eng*. 2016;115:12006. doi:10.1088/1757-899X/115/1/012006
69. Behera S, Gautam RK, Mohan S, Chattopadhyay A. Dry sliding Wear behavior of chemically treated sisal fiber reinforced epoxy composites. *J Nat Fibers*. 2022;19:6134-6147. doi:10.1080/15440478.2021.1904483
70. Yadav V, Singh S, Chaudhary N, et al. Dry sliding wear characteristics of natural fibre reinforced poly-lactic acid composites for engineering applications: fabrication, properties and characterizations. *J Mater Res Technol*. 2023;23:1189-1203. doi:10.1016/j.jmrt.2023.01.006
71. Kumar R, Anand A. Dry sliding friction and wear behavior of ramie fiber reinforced epoxy composites. *Mater Res Express*. 2018;6(1):15309. doi:10.1088/2053-1591/aae69b

SUPPORTING INFORMATION

Additional supporting information can be found online in the Supporting Information section at the end of this article.

How to cite this article: Shaisundaram VS, Sengottaiyan S, Mohan R, Gurunathan V. Assessment of mechanical, thermal, and sliding wear performance of chemically treated alumina-filled biocomposites using machine learning and response surface methodology. *Polym Compos*. 2025;1-19. doi:10.1002/pc.29798